Hindawi
Advances in Civil Engineering
Volume 2020, Article ID 8839400, 13 pages
https://doi.org/10.1155/2020/8839400

Research Article

Assessing the Risk Probability of the Embankment Seismic Damage Using Monte Carlo Method

Fa Che,[1,2] Chao Yin,[1,3] Han Zhang,[1] Gangting Tang,[1] Zhinan Hu,[4] Dong Liu,[5] Ying Li,[1] and Zhanfang Huang[1]

[1]*School of Civil and Architecture Engineering, Shandong University of Technology, Zibo, China*
[2]*Zibo Transportation Service Center, Zibo, China*
[3]*Key Laboratory of Roads and Railway Engineering Safety Control (Shijiazhuang Tiedao University), Ministry of Education, Shijiazhuang, China*
[4]*State Key Laboratory of Mechanical Behavior and System Safety of Traffic Engineering Structures (Shijiazhuang Tiedao University), Shijiazhuang, China*
[5]*Laoling Branch of Dezhou Highway Development Center, Dezhou, China*

Correspondence should be addressed to Chao Yin; yinchao1987611@163.com

Received 17 May 2020; Revised 20 August 2020; Accepted 8 September 2020; Published 21 September 2020

Academic Editor: Chunshun Zhang

There are few systematic studies on the risk probability assessment, although embankment seismic damages are extremely serious. Meanwhile, retaining walls and other retaining structures play positive roles in improving the embankment seismic performance, but relevant quantitative study is rarely reported. In particular, there are few existing studies on the seismic damage characteristics of the embankment fill-soil foundation system and the retaining structure-embankment fill-soil foundation system under different seismic actions. In view of this, the Xi'an-Baoji expressway K1125 + 470 embankment was taken as the research object, the risk probability assessment of the embankment seismic damage was conducted on the basis of the seismic fragility and seismic hazard assessment, the positive role of the retaining wall in improving the embankment seismic performance was verified, and the seismic damage evolution processes of the retaining wall-embankment fill-soil foundation system and the embankment fill-soil foundation system were analyzed. The research results show that the risk probabilities of the severe damage and destruction of the embankment fill-soil foundation system are 29.07% and 7.62% in the next 50 years, while of the retaining wall-embankment fill-soil foundation system are 19.30% and 3.46% and are reduced by 33.61% and 54.60%, respectively. The influence of the retaining wall on the embankment seismic performance mainly occurs at the middle stage of a violent earthquake, but the seismic damages of the retaining wall itself are also very serious, and the engineering disturbance of the retaining wall is reduced greatly or even lost completely at the final stage of the violent earthquake.

1. Introduction

Embankment is one of the most common structural forms of highway subgrade [1, 2]. In Tangshan earthquake, Wenchuan earthquake, Kyushu earthquake, East Japan earthquake, and other previous violent earthquakes, embankments suffered from varying degrees of damages, which seriously disrupted the highway networks [3–6]. It is greatly significant for improving the highway antiseismic capacity through proposing proper embankment reinforcement method on the basis of assessing the risk probability of the seismic damage [7–9]. The risk probability assessment is based on the seismic fragility assessment and seismic hazard assessment and analyzes their coupling characteristics. The assessment results can be represented by the risk probability exceeding each seismic damage level for a certain embankment in a future period of time [10–14].

Due to the increasing in frequencies and losses of earthquakes, researches on the risk probability assessment of the embankment seismic damage have attracted attention

from many scholars [15–19]. Enomoto and Sasaki [20] conducted a series of dynamic centrifuge model tests in order to evaluate some factors affecting the seismic performance of hillside embankments consisting of sandy or silty soils and resting on stiff base slope. Hutt et al. [21] benchmarked the antiseismic performance of a 50-story archetype office building designed following "Uniform Building Code (1973)" against "International Building Code (2015)" based on the seismic risk assessment. The mean annual frequency collapse risk of the 1973 building was 28 times greater than the equivalent 2015 building or approximately 13% versus 0.5% probability of collapse in 50 years. Liu et al. [22] performed the seismic fragility analysis of recycled aggregate concrete (RAC) bridge columns with different recycled coarse aggregate (RCA) replacement ratios subjected to freeze-thaw cycles (FTCs) by the cloud analysis method. Xu et al. [23] developed the Cumulative Absolute Velocity (CAV) with 24667 strong ground-motion records from Taiwan and the seismic hazard assessment for Taipei was then conducted using the local CAV models. Zanini et al. [24] proposed a framework for the development of seismic risk maps at nationwide scale. The seismic risk map was computed taking into account a *seismogenic* model of the analyzed area and properly characterizing vulnerability and exposure of an asset of interest. Scozzese et al. [25] analyzed the effectiveness of damping and isolation devices in mitigating the seismic risk by proposing a general framework for investigating the sensitivity of the seismic risk of structural systems with respect to system properties varying in a prescribed range. Bartoli et al. [26] analyzed the seismic risk of a confined historic masonry tower located in Italy and critically discussed the multilevel assessment path proposed by the "Italian Guidelines for the Assessment and Mitigation of the Seismic Risk of the Cultural Heritage." Risia et al. [27] studied how different procedures of site response analysis influence the risk quantification at urban scale and the risk was quantified in terms of direct losses incurred by the portfolio of buildings in Benevento for the 1980 Mw 6.9 Irpinia earthquake. Andreotti and Lai [28] proposed a comprehensive numerical methodology to construct fragility curves for mountain tunnels subjected to transversal seismic loading. The proposed numerical technique, which was based on fully nonlinear dynamic analyses accounting for the nonlinearity of both ground and tunnel support, allowed considering the features of the tunnel. Wang et al. [29] solved time-evolving probabilistic structural response through developed stochastic elastic-plastic finite element method (FEM); following that, formulation for seismic risk analysis was derived. Liu et al. [30] presented a novel perspective on scenario-based seismic vulnerability and hazard assessment; the findings could be a potential guide to decision-making in disaster risk reduction in rural Weinan (China). Maio et al. [31] aimed to investigate the correlation between two well-known approaches for the seismic risk assessment of stone masonry buildings located within historic centers: the vulnerability index method and nonlinear static seismic analyses. The latter were carried out by using a new three-dimensional macroelement model to numerically represent the considered sample of prototype buildings, together with the application of the N2 method. Castaldo and Alfano [32] developed incremental dynamic analyses to assess the seismic fragility considering several natural ground motions and different elastic and inelastic structural properties under the hypothesis of modeling the friction coefficients of the two surfaces of the double friction pendulum system (DFPS) as random variables.

There are few systematic studies on the hazard, fragility, and risk probability assessment, although the embankment seismic damages are extremely serious [11, 33]. Meanwhile, retaining walls and other retaining structures play positive roles in improving the embankment seismic performance, but relevant quantitative study is rarely reported [34]. In particular, there are few existing studies on the seismic damage characteristics of the embankment fill-soil foundation system and retaining structure-embankment fill-soil foundation system under different seismic actions [35]. In view of this, the Xi'an-Baoji expressway K1125 + 470 embankment was taken as the research object to assess the risk probability of the seismic damage and the positive influences of the retaining wall on reducing the risk probabilities were verified.

2. Embankment Seismic Fragility Assessment

2.1. Methodology. According to the differences in data acquisition and calculation method, the seismic fragility assessment is divided into empirical method and theoretical method [36, 37]. The theoretical method reflects the probabilistic relation between the seismic damage level and corresponding seismic ground-motion intensity through IDA and PSDA analysis [38, 39]. This method was adopted to assess the seismic fragility of the research object; the reasons are as follows [40–42].

2.1.1. Easy to Control Loading Levels. This method applies computer loading and can select different types and intensities of the seismic ground-motion records, thus completely reflecting the uncertainties of the ground-motions and reducing the influences of the subjective factors on the assessment results.

2.1.2. Realizing Quantitative Control of the Seismic Damage. Seismic damage levels can be output through software, avoiding the errors in judging the seismic damage levels by manual surveys, thus realizing quantitative control of the seismic damage.

2.1.3. Realizing Accurate Study on a Monomer Structure. Finite difference model of a monomer structure can be established by computer automatically, thus completely reflecting the antiseismic capacity of different structures and realizing accurate study on a monomer structure.

2.2. Data Preparation. By referencing on Castaldo et al. [43], the finite difference model of the embankment fill-soil foundation system of the research object was established by

adopting Flac software, wherein the vehicle loads were converted into the thickness of the embankment fill according to the elastic lamination theory [44, 45], as shown in Figure 1.

In modeling the embankment fill-soil foundation system, an elastoplastic constitutive relationship was employed, and the Mohr–Coulomb criterion was used as the yield criterion [43]. The mechanical properties of the embankment fill and soil foundation were determined as follows: shear modulus was 17.91 MPa and 15.67 MPa, respectively, density was 1970.00 kg/m^3 and 1630.00 kg/m^3, respectively, elastic modulus was 48.00 MPa and 42.00 MPa, respectively, Poisson's ratio was 0.34 and 0.36, respectively, bulk modulus was 50.00 MPa and 43.75 MPa, respectively, internal friction angle was 33.00° and 28.00°, respectively, and cohesive force was 34.00 KPa and 31.00 KPa, respectively [46, 47]. The drained conditions were not assumed.

Under the action of the ground acceleration $\ddot{u}_g$, the fundamental motion equation of the embankment fill-soil foundation system is shown in the following [48]:

$$M\ddot{u} + C\dot{u} + Ku = -MJ\ddot{u}_g, \tag{1}$$

where M refers to the total mass matrix containing the added vehicle mass, C refers to the total damping matrix, K refers to the total stiffness matrix, J refers to the indicator matrix of each seismic component, and $\ddot{u}$, $\dot{u}$, and u refer to the acceleration array, speed array, and displacement array of the nodes, respectively [49, 50]. The Rayleigh damping was selected as the model damping, PGA was selected as the seismic intensity parameter, and $\varepsilon_{\max}$ was selected as the seismic damage parameter, as shown in the following:

$$\varepsilon_{\max} = \frac{d_{\max}}{D}, \tag{2}$$

where $d_{\max}$ is the maximum lateral permanent displacement on the embankment surface and D is the embankment width. The reasons for selecting $\varepsilon_{\max}$ are as follows: (1) $\varepsilon_{\max}$ cannot only characterize the damage to the whole embankment, but also characterize the most vulnerable parts; (2) $\varepsilon_{\max}$ can reflect the seismic effect on traffic capacity: the larger the $\varepsilon_{\max}$ the more serious seismic damage and, therefore, the lower the traffic capacity. The corresponding relationship between the seismic damage level and $\varepsilon_{\max}$ was established on the basis of the displacement damage criterion, as shown in Table 1.

10 seismic ground-motion records provided by PEER for IDA analysis were selected [51]. The epicentral distance (E_d) of these records ranges from 11.7 km to 50.9 km, the magnitude (M_w) ranges from 6.0 to 7.6, and the original PGA ranges from 0.094 g to 0.714 g, as shown in Table 2.

Due to the limited space, the time-history curves of acceleration of the No. 1–No. 3 seismic ground-motion records are listed in Figure 2.

The PGA of each record was adjusted to 0.1 g, 0.2 g, 0.3 g, 0.4 g, 0.5 g, 0.6 g, 0.7 g, 0.8 g, 0.9 g, 1.0 g, 1.1 g, and 1.2 g, respectively [52], and obtained a total of 120 ground-motion records.

2.3. Embankment Seismic Fragility Assessment Results. The 120 seismic ground-motion records were input to the finite difference model shown in Figure 1, and 120 dynamic response analysis was undertaken [53, 54]. $\varepsilon_{\max}$ of each analysis as well as their mean value and standard deviation was computed, as shown in Table 3. The total energy dissipation of each analysis was also computed, as shown in Figure 3.

The logarithms of the PGA and $\varepsilon_{\max}$ were taken according to the dynamic response analysis results of the embankment fill-soil foundation system so as to obtain the probabilistic seismic demand model [32, 55, 56], as shown in the following:

$$\ln \varepsilon_{\max} = \ln 1.1396 + 1.1821 \ln \mathrm{PGA}. \tag{3}$$

Formula (3) was substituted into the classical calculation formula of the seismic fragility to obtain the following:

$$P_j = \Phi\left(2 \cdot \ln \frac{1.1396\mathrm{PGA}^{1.1821}}{S_j}\right), \tag{4}$$

where P_j refers to the exceeding probability of the embankment seismic damage level j and $j = 1$ represents basically intact, $j = 2$ represents slight damage, $j = 3$ represents moderate damage, $j = 4$ represents severe damage, $j = 5$ represents destruction, and S_j refers to the structural performance level shown in Table 1, namely, $S_2 = 0.20$ when $j = 2$, $S_3 = 0.40$ when $j = 3$, $S_4 = 0.80$ when $j = 4$, and $S_5 = 1.20$ when $j = 5$. The embankment seismic fragility curves were plotted according to formula (4), as shown in Figure 4.

The exceeding probability of each seismic damage level of the embankment fill-soil foundation system was calculated according to Figure 4, as shown in Table 4. The exceeding probabilities of the severe damage and destruction are 0.760416 and 0.458867 when PGA = 1.0 g, respectively, which are basically consistent with the survey results of the embankment seismic damage near the epicenter of the Wenchuan earthquake (PGA = 0.977 g) and further show that the embankment seismic fragility assessment method adopted in this paper is scientific and rational.

3. Risk Probability Assessment of the Embankment Seismic Damage

3.1. Methodology. Risk probability of the embankment seismic damage numerically equals the convolution between the seismic hazard of the site and the embankment seismic fragility, that is, the integral of exceeding probabilities of all damage levels under all seismic events in the next t years [57], as shown in the following:

$$P_{j,t} = \int_{R_{j-}}^{\infty} f_t(S)\mathrm{d}S, \tag{5}$$

where Pj,t refers to the risk probability exceeding the seismic damage level j in the next t years and $ft(S)$ refers to the probability density function of the comprehensive effect on the embankment from the risk events, that is, the probability

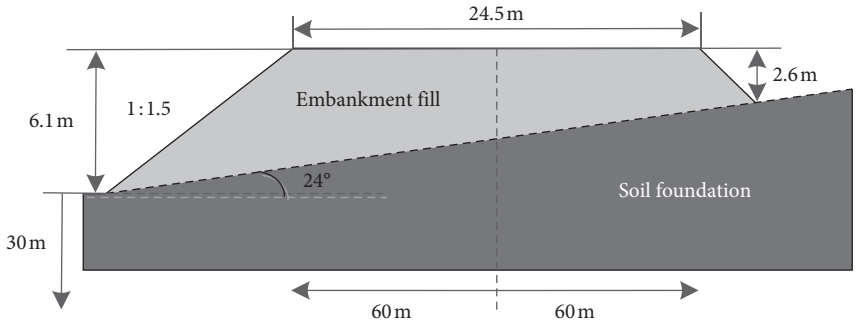

Figure 1: Finite difference model of the embankment fill-soil foundation system.

Table 1: Relationship between the seismic damage level and ε_{max}.

Seismic damage level	Basically intact	Slight damage	Moderate damage	Severe damage	Destruction
ε_{max}	$0 \le \varepsilon_{max} < 0.20$	$0.20 \le \varepsilon_{max} < 0.40$	$0.40 \le \varepsilon_{max} < 0.80$	$0.80 \le \varepsilon_{max} < 1.20$	$\varepsilon_{max} \ge 1.20$

Table 2: Selected seismic ground-motion records.

Sequence number	Earthquake	E_d	M_w	Original PGA (g)
1	Kobe_Japan	49.9	6.9	0.094
2	Landers	50.9	7.3	0.117
3	San Simeon_CA	38.0	6.5	0.132
4	Duzce_Turkey	34.3	7.1	0.138
5	Chalfont Valley-1	16.2	6.0	0.248
6	Cape Mendocino	18.5	7.1	0.385
7	Chalfont Valley-2	11.7	6.0	0.447
8	Cape Mendocino	13.5	7.1	0.591
9	Chi-Chi, Taiwan-1	26.0	7.6	0.639 g
10	Chi-Chi, Taiwan-2	18.8	7.6	0.724 g

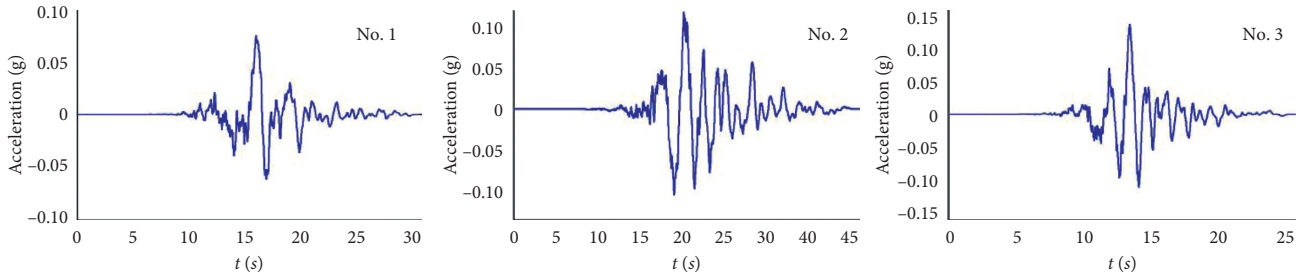

Figure 2: Time-history curves of acceleration of the No. 1–No. 4 seismic ground-motion records.

density function of the values of ε_{max} in the next t years [58]. The calculation method of $ft(S)$ is shown in the following:

$$f_t(S) = f(S \mid E) f_t(E), \tag{6}$$

where E refers to the earthquake event and $f(S\,E)$ refers to the conditional probability density of ε_{max} under any given E, that is, the results of the embankment seismic fragility assessment. $Ft(E)$ refers to the probability density function of the seismic event, that is, PGA distribution model of the embankment site, being results of the seismic hazard assessment [59]. According to (5) and (6), the calculation method of Pj,t is shown in the following:

$$P_{j,t} = P_{j,t}\left(R_{j-} \le S\right) = \int_{R_{j-}}^{\infty} \int_{0}^{\infty} f(S \mid E) f_t(E) \mathrm{d}E \mathrm{d}S. \tag{7}$$

3.2. Seismic Ground-Motion Distribution Model. Seismic ground-motion distribution model includes the probability distribution model of the site seismic intensity and transformational relationship between the seismic intensity and PGA.

3.2.1. Probability Distribution Model of the Site Seismic Intensity. Liu and Zhang [60] analyzed the seismic hazard

Table 3: Dynamic response analysis results.

PGA (g)	ε_{max} Sequence number of the seismic ground-motion records										Mean value	Standard deviation
	No. 1	No. 2	No. 3	No. 4	No. 5	No. 6	No. 7	No. 8	No. 9	No. 10		
0.1	0.0795	0.0774	0.0751	0.0695	0.0754	0.0681	0.0622	0.0574	0.0702	0.0635	0.0698	0.0072
0.2	0.1579	0.1629	0.1964	0.1854	0.1788	0.1763	0.1844	0.1924	0.1605	0.1864	0.1781	0.0136
0.3	0.2549	0.2678	0.2845	0.2789	0.2657	0.2458	0.2987	0.2697	0.2784	0.2567	0.2701	0.0156
0.4	0.3568	0.3459	0.4103	0.3746	0.4472	0.3521	0.3854	0.4086	0.3795	0.4187	0.3879	0.0328
0.5	0.4983	0.4909	0.4352	0.4651	0.5029	0.4901	0.5418	0.5065	0.4587	0.4952	0.4885	0.0294
0.6	0.5868	0.5698	0.5717	0.5329	0.5324	0.6487	0.5349	0.6173	0.5551	0.5837	0.5733	0.0381
0.7	0.7964	0.7542	0.7781	0.7045	0.7954	0.7745	0.7542	0.7267	0.7524	0.7854	0.7622	0.0299
0.8	0.7534	0.8637	0.8525	0.7201	0.7968	0.7716	0.8055	0.7784	0.7738	0.7719	0.7888	0.0433
0.9	0.9027	1.0587	0.9627	0.9984	0.9578	0.9057	0.9254	0.9742	0.9781	1.0485	0.9712	0.0535
1.0	1.2694	1.1458	1.3694	1.1129	1.2287	1.1567	1.3042	1.1964	1.2023	1.0894	1.2075	0.0877
1.1	1.3695	1.3384	1.3145	1.3075	1.2827	1.2984	1.2645	1.3064	1.3275	1.2287	1.3038	0.0393
1.2	1.5843	1.4134	1.5436	1.5756	1.5149	1.5084	1.4371	1.6294	1.5555	1.5156	1.5278	0.0657

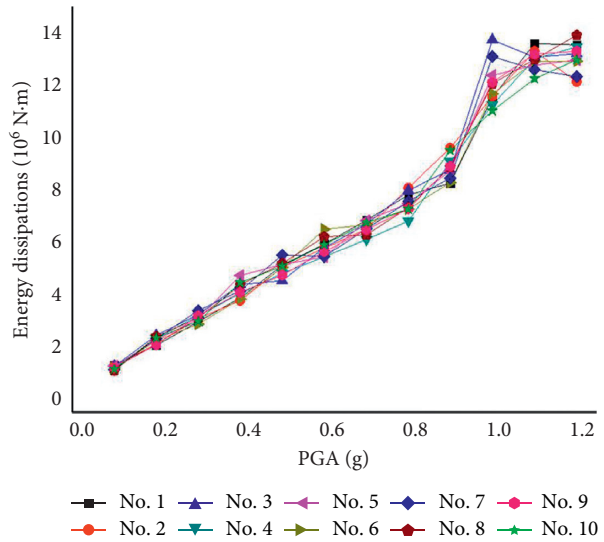

Figure 3: Total energy dissipations of the embankment fill-soil foundation system.

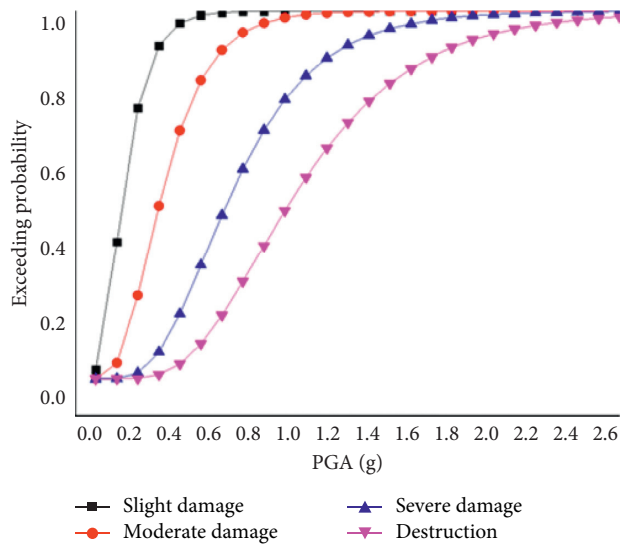

Figure 4: Seismic fragility curves of the embankment fill-soil foundation system.

Table 4: Seismic fragility assessment results of the embankment fill-soil foundation system.

PGA	Exceeding probability			
	Slight damage	Moderate damage	Severe damage	Destruction
0.1	0.024792	0.000404	0.000000	0.000000
0.2	0.372665	0.043532	0.000976	0.000005
0.3	0.736894	0.225876	0.016226	0.001590
0.4	0.905566	0.471158	0.072330	0.011616
0.5	0.967225	0.675516	0.175902	0.040752
0.6	0.988473	0.812256	0.308519	0.094932
0.7	0.995818	0.894475	0.446065	0.171937
0.8	0.998425	0.941370	0.571457	0.264071
0.9	0.999384	0.967470	0.676721	0.362276
1.0	0.999750	0.981867	0.760416	0.458867
1.1	0.999895	0.989810	0.824583	0.548568
1.2	0.999954	0.994215	0.872583	0.628452
1.3	0.999979	0.996678	0.907898	0.697420
1.4	0.999990	0.998070	0.933597	0.755594
1.5	0.999995	0.998865	0.952167	0.803811
1.6	0.999998	0.999325	0.965531	0.843247
1.7	0.999999	0.999594	0.975128	0.875180
1.8	0.999999	0.999753	0.982016	0.900841
1.9	1.000000	0.999848	0.986963	0.921346
2.0	1.000000	0.999905	0.990522	0.937663
2.1	1.000000	0.999940	0.993087	0.950610
2.2	1.000000	0.999962	0.994940	0.960862
2.3	1.000000	0.999976	0.996284	0.968971
2.4	1.000000	0.999984	0.997260	0.975379
2.5	1.000000	0.999990	0.997973	0.980444
2.6	1.000000	0.999993	0.998495	0.984448

assessment results of dozens of sites in the "Three North Areas" in China. According to the results, the seismic intensities of a certain site in the next 50 years comply with the extreme value type (III) distribution; the distribution function is shown in the following:

$$F(x) = \exp\left[-\left(\frac{\omega - x}{\omega - \varepsilon}\right)^K\right], \tag{8}$$

where ω refers to the maximum seismic intensity value. According to China's current seismic intensity

classification method, $\omega = 12$. ε refers to the normal seismic intensity, that is, the seismic intensity with exceeding probability of 63% in the next 50 years. K refers to the shape parameter, which can be determined by 3 methods, that is, fractile method, least square method, and maximum likelihood method [61]. From the view of accuracy of fitting, the least square method is optimal; however, the K value corresponding to the basic seismic intensity (exceeding probability of 10% in the next 50 years) can satisfy the requirements from the view of engineering practice [62].

According to (8), the probability distribution function of the site seismic intensity in the next t years is shown in the following:

$$F_t(x) = \exp\left[-\left(\frac{\omega - x}{\omega - \varepsilon}\right)^K\right]^{t/50} = \exp\left[-\frac{t}{50}\left(\frac{\omega - x}{\omega - \varepsilon}\right)^K\right]. \tag{9}$$

Taking the derivative of (9), the probability density function of the site seismic intensity in the next t years was obtained, as shown in the following:

$$f_t(x) = \frac{tK(\omega - x)^{K-1}}{50(\omega - \varepsilon)} \exp\left[-\frac{t}{50}\left(\frac{\omega - x}{\omega - \varepsilon}\right)^K\right]. \tag{10}$$

3.2.2. Transformational Relationship between the Seismic Intensity and PGA. The transformational relationship between the seismic intensity and PGA proposed by Liu and Zhang [60] was adopted in this paper, as shown in the following:

$$\mathrm{PGA} = 10I^{\lg 2 - 0.01}. \tag{11}$$

where I refers to the seismic intensity. Although the seismic intensity values are integer discrete variables between 1 and 12, in consideration of the calculation accuracy and model applicability, the seismic intensity values in (11) are considered as continuous variables.

3.3. Risk Probability Assessment Based on the Monte Carlo Method. According to (3), (10), and (11), complicated integral operations will be inevitably conducted when the numerical method is directly applied to calculate the risk probability, and convergence in the field of integral cannot be guaranteed. Therefore, the Monte Carlo method was applied to assess the risk probability of the embankment seismic damage.

3.3.1. Basic Idea. MATLAB software was used to conduct n times of sampling for the seismic intensity based on (10). The seismic intensity and PGA were transformed based on (11); then, the occurrence probability of an individual PGA in overall samples was $1/n$. $Pj(\mathrm{PGA}i)$ was defined as the risk probability exceeding the seismic damage level j under the action of PGAi, which can be calculated based on the fragility assessment results. When n is large enough, (7) can be changed to (12) according to the law of large numbers [63, 64].

$$P_{j,t} = P_{j,t}\left(R_{j-} \le S\right) = \frac{1}{n}\sum_{i=1}^{n} N\left(R_{j-} \le S_i\right) = \frac{1}{n}\sum_{i=1}^{n} P_j\left(\mathrm{PGA}_i\right), \tag{12}$$

where $N(R_{j\text{-}} \le S_i) = 1$ when $R_{j\text{-}} \le S_i$ and $N(R_{j\text{-}} \le S_i) = 0$ when $R_{j\text{-}} > S_i$.

3.3.2. Case Study. According to the seismic hazard assessment results along the Xi'an-Baoji expressway, PGAs with certain exceeding probabilities in the next 50 years were calculated [11]. According to (11), the corresponding seismic intensities were calculated, as shown in Table 5.

According to Table 5 and Figure 5, the shape parameter K was determined based on the seismic intensities with exceeding probabilities of 10% and 63% in the next 50 years, as shown in the following:

$$0.9 = \exp\left[-\left(\frac{12 - 7.705}{12 - 6.385}\right)^K\right] = \exp\left[-\left(\frac{4.295}{5.615}\right)^K\right]. \tag{13}$$

The solution is $K = 8.397$. The probability distribution of the seismic intensity of the embankment site in the next 50 years is shown in the following formula and Figure 6.

$$F(x) = \exp\left[-\left(\frac{12 - x}{5.615}\right)^{8.397}\right]. \tag{14}$$

Taking the derivative of Formula (14), the probability density of the seismic intensity of the embankment site in the next 50 years is shown in the following formula and Figure 7.

$$f(x) = \frac{8.397(12 - x)^{7.397}}{5.615^{8.397}} \exp\left[-\left(\frac{12 - x}{5.615}\right)^{8.397}\right]. \tag{15}$$

In consideration of the calculation accuracy and model applicability, the best results can be obtained when the number of simulations is 100000 when the Monte Carlo method is conducted [65]. According to the probability density of the seismic intensity of the embankment site shown in Formula (15), the MATLAB software was used in sampling and 100000 random numbers I_1, I_2, I_3, ……, I_{100000} were selected, which indicated the 100000 possibilities of the seismic intensities; besides, the above random numbers complied with the seismic hazard assessment results. After inputting I_1, I_2, I_3, ……, I_{100000} to Formula (11), 100000 possible PGAs of the embankment site in the next 50 years PGA_1, PGA_2, PGA_3, ……, PGA_{100000} were calculated.

According to Figure 3, $P_2(\mathrm{PGA}_1)$, $P_2(\mathrm{PGA}_2)$, $P_2(\mathrm{PGA}_3)$,…, $P_2(\mathrm{PGA}_{100000})$ are defined as the exceeding probabilities of the slight damage under the actions of PGA_1, PGA_2, PGA_3,…, PGA_{100000}, respectively. The risk probability exceeding the slight damage in the next 50 years $P_{2,50}$ was calculated according to Formula (13), as shown in the following:

Table 5: Seismic intensities in the next 50 years.

Exceeding probability (%)	2	10	63
PGA (g)	0.3155	0.2106	0.0851
Seismic intensity	8.293	7.705	6.385

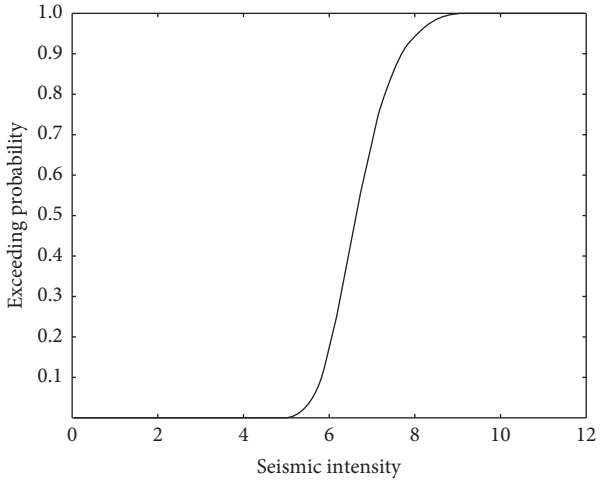

Figure 5: Structure form of the retaining wall-embankment fill-soil foundation system.

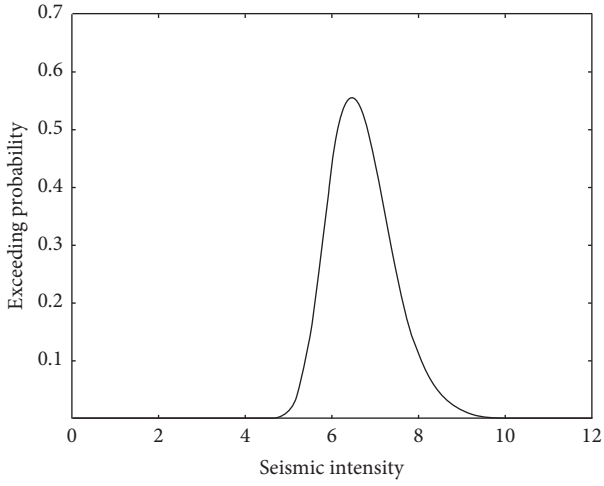

Figure 6: Probability distribution of the seismic intensity of the embankment site in the next 50 years' embankment.

$$P_{2,50} = \sum_{i=1}^{100000} \frac{P_2(\mathrm{PGA}_i)}{100000}. \quad (16)$$

$P2{,}50 = 98.22\%$ was calculated according to Formula (16). Similarly, $P3{,}50 = 68.03\%$, $P4{,}50 = 29.07\%$, and $P5{,}50 = 7.62\%$. On this basis, the risk probability of each seismic damage level in the next 50 years was calculated, respectively, according to the following formula, as shown in Table 6.

$$\begin{cases} D_{j,50} = P_{j,50} \quad (j = 5), \\ D_{j,50} = P_{j,50} - P_{j+1,50} \quad (j = 1, 2, 3, 4), \end{cases} \quad (17)$$

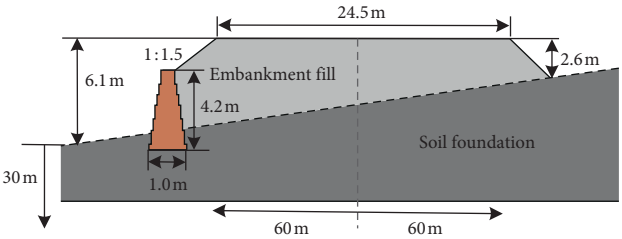

Figure 7: Probability density of the seismic intensity of the embankment site in the next 50 years' embankment.

where $D_{j,50}$ refers to the risk probability of each seismic damage level in the next 50 years.

4. Discussion

4.1. Risk Probability Assessment Results of the Retaining Wall-Embankment Fill-Soil Foundation System. In order to verify the positive influences of the retaining wall on the risk probability of the embankment seismic damage, a retaining wall was assumed to be built at the left side of the research object. An isotropic elastic constitutive relationship was used to model the retaining wall, and the mechanical properties were: elastic modulus 3000.00 MPa, Poisson's ratio 0.17, bulk modulus 1515.15 MPa, shear modulus 1282.05 MPa, and density 2300.00 kg/m^3 (Yin et al. [11]), and the structural form of the retaining wall-embankment fill-soil foundation system is shown in Figure 5.

120 dynamic response analysis were conducted on the retaining wall-embankment fill-soil foundation system. The total energy dissipation of each analysis is shown in Figure 8, the fragility curves are shown in Figure 9, the assessment results are shown in Tables 7 and 8.

It can be seen that the risk probability of the embankment seismic damage can be significantly reduced through the retaining wall; for example, the risk probabilities of the severe damage and destruction of the retaining wall-embankment fill-soil foundation system are 29.07% and 7.62%, while risk probabilities of the embankment fill-soil foundation system are 19.30% and 3.46% and there is a reduction of 33.61% and 54.60%, respectively.

4.2. Influences of the Retaining Wall on the Embankment Seismic Damages. Figure 10 lists the seismic damages of the embankment fill-soil foundation system and the retaining wall-embankment fill-soil foundation system under the actions of No. 1 seismic ground-motions when PGA = 0.2 g, 0.4 g, 0.6 g, 0.8 g, 1.0 g, and 1.2 g, respectively.

It can be seen from Figure 10 that the seismic damages mainly include cracks and lateral displacement on the top surface of the embankment fill, wherein the damages of the retaining wall-embankment fill-soil foundation system are obviously lower than those of the embankment fill-soil foundation system; namely, the $\varepsilon_{\max}$ is reduced by 18.11% and the crack length is shortened by 21.83% on average. However, the seismic damages of the retaining wall itself are also very serious; especially after a violent earthquake, the

Table 6: Risk probability assessment results.

Seismic damage level	Basically intact	Slight damage (%)	Moderate damage (%)	Severe damage (%)	Destruction (%)
Risk probability exceeding each damage level	100.00	98.22	68.03	29.07	7.62
Risk probability of each damage level	1.78	30.19	38.96	21.45	7.62

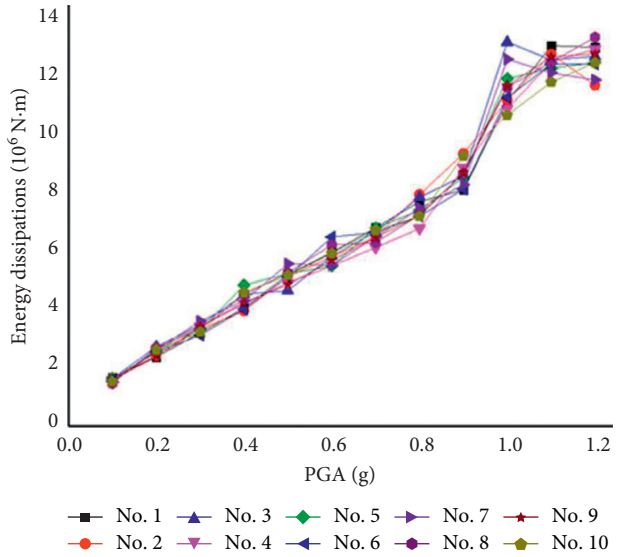

Figure 8: Total energy dissipation of the retaining wall-embankment fill-soil foundation system fill-soil foundation system.

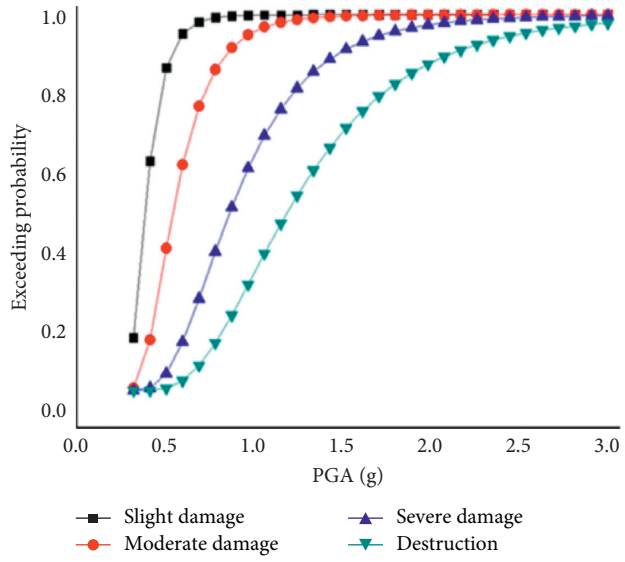

Figure 9: Fragility curves of the retaining wall-embankment fill-soil foundation system fill-soil foundation system.

engineering disturbance of the retaining wall is reduced greatly or even lost completely.

Figure 11 lists the seismic damage evolution processes of the embankment fill-soil foundation system and the retaining wall-embankment fill-soil foundation system under the action of No. 1 seismic ground-motion when

Table 7: Fragility assessment results of the retaining wall-embankment fill-soil foundation system.

PGA (g)	Exceeding probability			
	Slight damage	Moderate damage	Severe damage	Destruction
0.1	0.139971	0.006817	0.000005	0.000001
0.2	0.610763	0.134583	0.006364	0.000480
0.3	0.859458	0.378886	0.045066	0.006112
0.4	0.949815	0.601322	0.129339	0.026162
0.5	0.981304	0.756522	0.244740	0.066540
0.6	0.992649	0.853909	0.369587	0.126337
0.7	0.996951	0.912481	0.487993	0.200165
0.8	0.998671	0.947226	0.591822	0.281397
0.9	0.999394	0.967838	0.678544	0.364183
1.0	0.999713	0.980153	0.748769	0.444208
1.1	0.999859	0.987589	0.804517	0.518719
1.2	0.999928	0.992135	0.848216	0.586239
1.3	0.999962	0.994950	0.882201	0.646219
1.4	0.999980	0.996716	0.908513	0.698721
1.5	0.999989	0.997838	0.928839	0.744174
1.6	0.999994	0.99856	0.944531	0.783204
1.7	0.999996	0.99903	0.956652	0.816515
1.8	0.999998	0.99934	0.966029	0.844818
1.9	0.999999	0.999547	0.973296	0.868787
2.0	0.999999	0.999685	0.978942	0.889042
2.1	1.000000	0.99978	0.983341	0.906131
2.2	1.000000	0.999844	0.986778	0.920537
2.3	1.000000	0.999889	0.989471	0.932676
2.4	1.000000	0.999921	0.991589	0.942905
2.5	1.000000	0.999943	0.993259	0.951526
2.6	1.000000	0.999958	0.994580	0.958797
2.7	1.000000	0.999969	0.995629	0.964932
2.8	1.000000	0.999977	0.996464	0.970115
2.9	1.000000	0.999983	0.997131	0.974497
3.0	1.000000	0.999988	0.997665	0.978206

PGA = 1.2 g, it can be seen that the differences of the seismic damages between the two systems are not obvious at the initial stage of a violent earthquake ($t = 2$ s and 4 s). The seismic damage of the retaining wall-embankment fill-soil foundation system is obviously lower than that of the embankment fill-soil foundation system since the retaining wall bears larger passive Earth pressure at the middle stage of a violent earthquake ($t = 6$ s and 8 s). At the final stage of a violent earthquake ($t = 10$ s and 12 s), the seismic damage of the retaining wall is increased and the passive Earth pressure is reduced with continuous development of the cracks and lateral displacement on the top surface of the embankment fill, and the seismic damage increasing range of the retaining wall-embankment fill-soil foundation system is basically consistent with that of the embankment fill-soil foundation system.

Table 8: Risk probability assessment results of the retaining wall-embankment fill-soil foundation system.

Seismic damage level	Basically intact (%)	Slight damage (%)	Moderate damage (%)	Severe damage (%)	Destruction (%)
Risk probability exceeding each damage level	100.00	59.37	52.79	19.30	3.46
Risk probability of each damage level	10.63	36.58	33.49	15.84	3.46

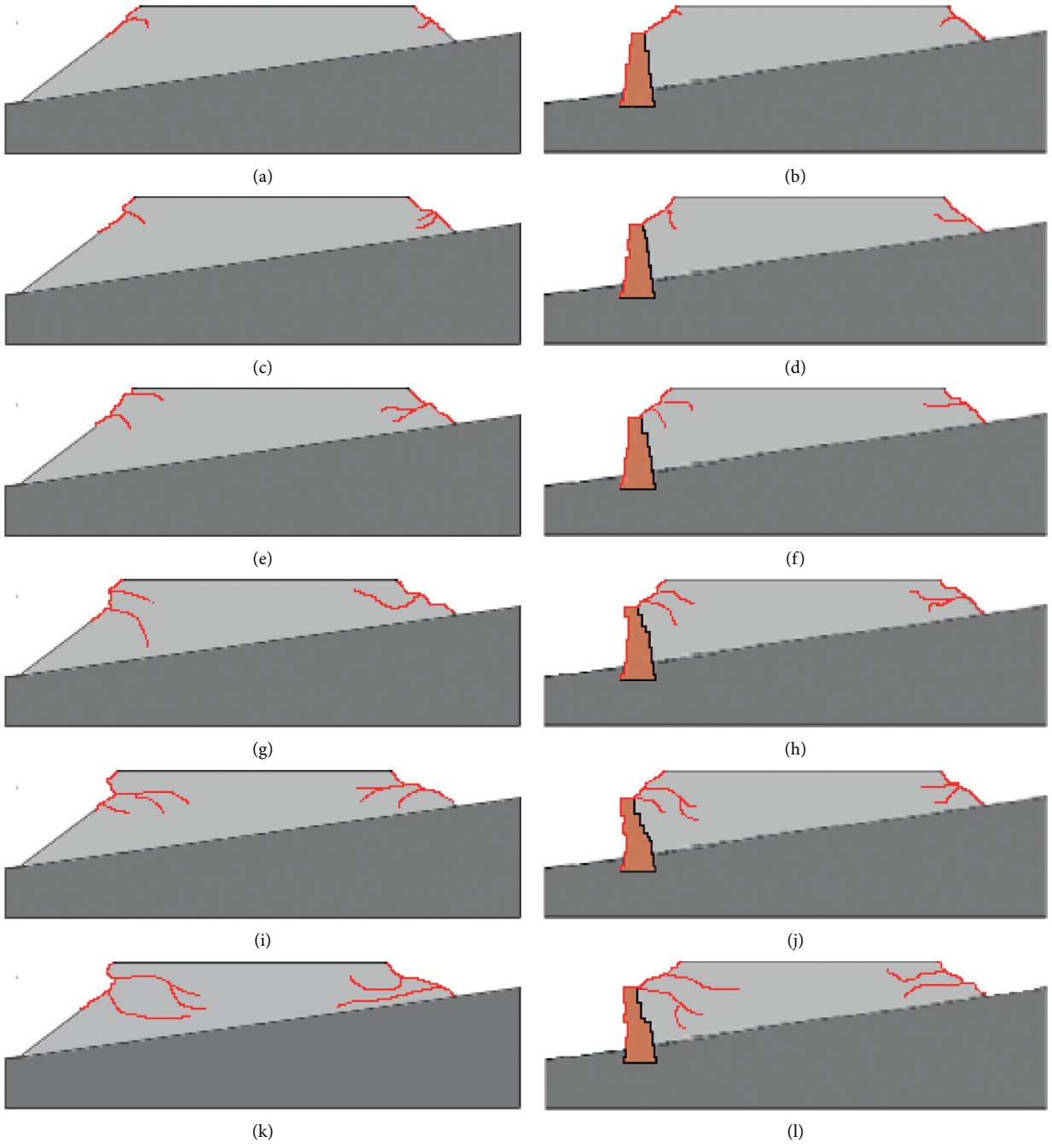

Figure 10: Embankment seismic damages. (a) Embankment fill-soil foundation system, PGA = 0.2 g, $\varepsilon_{max} = 0.1579$, and crack length is 2.38 m. (b) Retaining wall-embankment fill-soil foundation system, PGA = 0.2 g, $\varepsilon_{max} = 0.1195$, and crack length is 1.92 m. (c) Embankment fill-soil foundation system, PGA = 0.4 g, $\varepsilon_{max} = 0.3568$, and crack length is 3.71 m. (d) Retaining wall-embankment fill-soil foundation system, PGA = 0.4 g, $\varepsilon_{max} = 0.2954$, and crack length is 3.08 m. (e) Embankment fill-soil foundation system, PGA = 0.6 g, $\varepsilon_{max} = 0.5868$, and crack length is 6.49 m. (f) Retaining wall-embankment fill-soil foundation system, PGA = 0.6 g, $\varepsilon_{max} = 0.4938$, and crack length is 4.18 m. (g) Embankment fill-soil foundation system, PGA = 0.8 g, $\varepsilon_{max} = 0.7534$, and crack length is 12.86 m. (h) Retaining wall-embankment fill-soil foundation system, PGA = 0.8 g, $\varepsilon_{max} = 0.6382$, and crack length is 10.34 m. (i) Embankment fill-soil foundation system, PGA = 1.0 g, $\varepsilon_{max} = 1.2694$, and crack length is 16.32 m. (j) Retaining wall-embankment fill-soil foundation system, PGA = 1.0 g, $\varepsilon_{max} = 0.9541$, and crack length is 12.21 m. (k) Embankment fill-soil foundation system, PGA = 1.2 g, $\varepsilon_{max} = 1.5843$, and crack length is 24.84 m. (l) Retaining wall-embankment fill-soil foundation system, PGA = 1.2 g, $\varepsilon_{max} = 1.3548$, and crack length is 20.33 m.

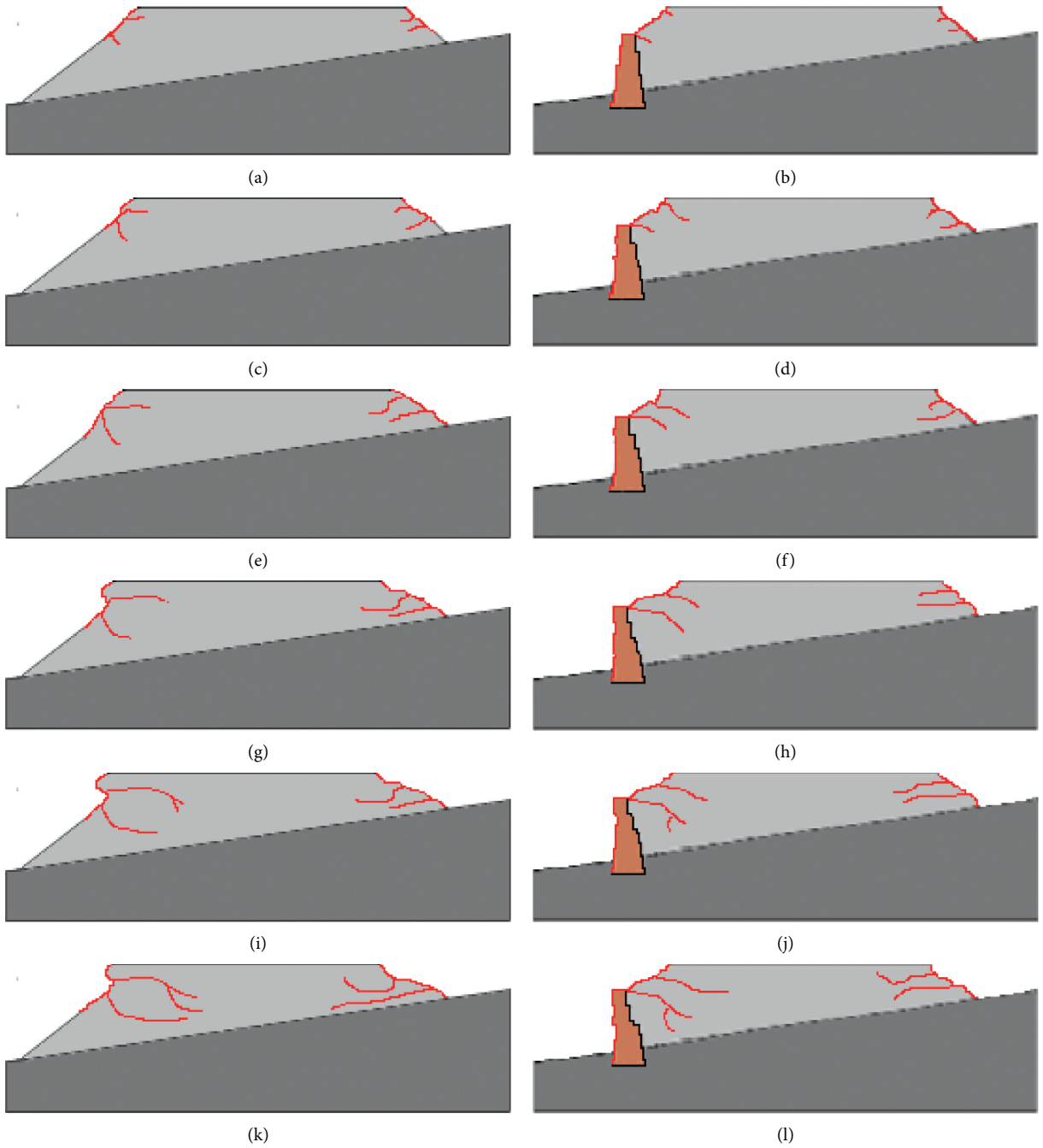

FIGURE 11: Seismic damage evolution processes. (a) Embankment fill-soil foundation system, $t = 2$ s, $\varepsilon_{max} = 0.0927$, and crack length is 1.24 m. (b) Retaining wall-embankment fill-soil foundation system, $t = 2$ s, $\varepsilon_{max} = 0.0854$, and crack length is 1.19 m. (c) Embankment fill-soil foundation system, $t = 4$ s, $\varepsilon_{max} = 0.3264$, and crack length is 5.37 m. (d) Retaining wall-embankment fill-soil foundation system, $t = 4$ s, $\varepsilon_{max} = 0.3004$, and crack length is 5.12 m. (e) Embankment fill-soil foundation system, $t = 6$ s, $\varepsilon_{max} = 0.5846$, and crack length is 9.67 m. (f) Retaining wall-embankment fill-soil foundation system, $t = 6$ s, $\varepsilon_{max} = 0.4237$, and crack length is 7.51 m. (g) Embankment fill-soil foundation system, $t = 8$ s, $\varepsilon_{max} = 0.8064$, and crack length is 15.85 m. (h) Retaining wall-embankment fill-soil foundation system, $t = 8$ s, $\varepsilon_{max} = 0.5932$, and crack length is 11.24 m. (i) Embankment fill-soil foundation system, $t = 10$ s, $\varepsilon_{max} = 1.2982$, and crack length is 20.37 m. (j) Retaining wall-embankment fill-soil foundation system, $t = 10$ s, $\varepsilon_{max} = 0.9567$, and crack length is 16.58 m. (k) Embankment fill-soil foundation system, $t = 12$ s, $\varepsilon_{max} = 1.5843$, and crack length is 24.84 m. (l) Retaining wall-embankment fill-soil foundation system, $t = 12$ s, $\varepsilon_{max} = 1.3548$, and crack length is 20.33 m.

5. Conclusions

(1) The Xi'an-Baoji expressway K1125 + 470 embankment was taken as the research object, the risk probability assessment of the embankment seismic damage was conducted on the basis of the seismic fragility and seismic hazard assessment, the positive role of the retaining wall in improving the embankment seismic performance was verified, and the seismic damage evolution processes of the retaining wall-embankment fill-soil foundation system and the embankment fill-soil foundation system were analyzed.

(2) The risk probabilities of the severe damage and destruction of the embankment fill-soil foundation system are 29.07% and 7.62% in the next 50 years, while those of the retaining wall-embankment fill-soil foundation system are 19.30% and 3.46% and are reduced by 33.61% and 54.60%, respectively. The influence of the retaining wall on the embankment seismic performance mainly occurs at the middle stage of a violent earthquake, but the seismic damages of the retaining wall itself are also very serious, and the engineering disturbance of the retaining wall is reduced greatly, or even lost completely at the final stage of the violent earthquake.

(3) The research results can be used as the theoretical basis of the embankment antiseismic design, and the proposed risk probability assessment method can also be applied to similar structures. However, some aspects of this paper can be further improved; for example, the study on the dynamic coupling mechanism of the embankment and the seismic ground-motion can continue to be developed in the future.

Data Availability

The data used to support the findings of this study are available from the corresponding author upon request.

Conflicts of Interest

The authors declare that they have no conflicts of interest with respect to the research, authorship, and publication of this article.

Acknowledgments

This research was supported by the National Natural Science Foundation of China (Grant no. 51808327) and Natural Science Foundation of Shandong Province (Grant no. ZR2019PEE016).

References

[1] E. N. S. Klimis, "Exploring the interplay between normal fault rupture and a highway embankment founded on a single-layered soil: mapping and quantification of damage," *Soil Dynamics and Earthquake Engineering*, vol. 123, pp. 91–109, 2019.

[2] L. Liu, Z. Li, G. Cai, X. Liu, and S. Yan, "Humidity field characteristics in road embankment constructed with recycled construction wastes," *Journal of Cleaner Production*, vol. 259, Article ID 120977, 2020.

[3] C. Xu, J. Deng, S. Peng, and C. Li, "Seismic fragility analysis of steel reinforced concrete frame structures based on different engineering demand parameters," *Journal of Building Engineering*, vol. 20, pp. 736–749, 2018.

[4] T. Enomoto and T. Sasaki, "Seismic behaviour of reinforced embankments in dynamic centrifuge model tests," *Soils and Foundations*, vol. 58, no. 1, pp. 212–227, 2018.

[5] G. Modoni, M. Albano, E. Salvatore, and J. Koseki, "Effects of compaction on the seismic performance of embankments built with gravel," *Soil Dynamics and Earthquake Engineering*, vol. 106, pp. 231–242, 2018.

[6] J. Ma, X. J. Feng, G. Y. Li, and X. N. Li, "New insights from analysis of historical texts on the 1568 Northeast Xi'an earthquake, Shaanxi, China," *International Journal of Disaster Risk Reduction*, vol. 44, Article ID 101417, 2020.

[7] N. Xiang, Y. Goto, M. Obata, and M. S. Alam, "Passive seismic unseating prevention strategies implemented in highway bridges: a state-of-the-art review," *Engineering Structures*, vol. 194, pp. 77–93, 2019.

[8] C. Xiong, Q. Li, and X. Lu, "Automated regional seismic damage assessment of buildings using an unmanned aerial vehicle and a convolutional neural network," *Automation in Construction*, vol. 109, Article ID 102994, 2020.

[9] S. Yang, Y. Gao, B. Leshchinsky, K. Cui, and F. Zhang, "Internal stability analysis of reinforced convex highway embankments considering seismic loading," *Geotextiles and Geomembranes*, vol. 48, no. 3, pp. 221–229, 2020.

[10] M. Shokrabadi and H. V. Burton, "Regional short-term and long-term risk and loss assessment under sequential seismic events," *Engineering Structures*, vol. 185, pp. 366–376, 2019.

[11] C. Yin, Y. Li, and F.-F. Liu, "Probability risk assessment and management of embankment seismic damages based on CPSHA-PSDA," *Iranian Journal of Science and Technology, Transactions A: Science*, vol. 43, no. 4, pp. 1563–1574, 2019.

[12] Z. Geng, H. Wang, M. Fan et al., "Predicting seismic-based risk of lost circulation using machine learning," *Journal of Petroleum Science and Engineering*, vol. 176, pp. 679–688, 2019.

[13] M. Vona, "A novel approach to improve the code provision based on a seismic risk index for existing buildings," *Journal of Building Engineering*, vol. 28, Article ID 101037, 2020.

[14] D. Perrone, G. J. O'Reilly, R. Monteiro, and A. Filiatrault, "Assessing seismic risk in typical Italian school buildings: from in-situ survey to loss estimation," *International Journal of Disaster Risk Reduction*, vol. 44, Article ID 101448, 2020.

[15] R. Pang, B. Xu, X. Kong, and D. Zou, "Seismic fragility for high CFRDs based on deformation and damage index through incremental dynamic analysis," *Soil Dynamics and Earthquake Engineering*, vol. 104, pp. 432–436, 2018.

[16] D.-S. Ling, Y. Zhao, B. Huang, F. Zhang, and Y. Zhou, "Analysis of dynamic stress path in inhomogenous subgrade under moving aircraft load," *Soil Dynamics and Earthquake Engineering*, vol. 111, pp. 65–76, 2018.

[17] Y. Xie and R. Desroches, "Sensitivity of seismic demands and fragility estimates of a typical California highway bridge to uncertainties in its soil-structure interaction modeling," *Engineering Structures*, vol. 189, pp. 605–617, 2019.

[18] J. Zhou, S. Li, G. Nie, X. Fan, Y. Deng, and C. Xia, "Research on seismic vulnerability of buildings and seismic disaster risk: a case study in Yancheng, China," *International Journal of Disaster Risk Reduction*, vol. 45, Article ID 101477, 2020.

[19] N. M. Campbell, M. Leon-Corwin, L. A. Ritchie, and J. Vickery, "Human-induced seismicity: risk perceptions in the state of Oklahoma," *The Extractive Industries and Society*, vol. 7, no. 1, pp. 119–126, 2020.

[20] T. Enomoto and T. Sasaki, "Several factors affecting seismic behaviour of embankments in dynamic centrifuge model tests," *Soils and Foundations*, vol. 55, no. 4, pp. 813–828, 2015.

[21] C. M. Hutt, T. Rossetto, and G. G. Deierlein, "Comparative risk-based seismic assessment of 1970s vs modern tall steel moment frames," *Journal of Constructional Steel Research*, vol. 159, pp. 598–610, 2019.

[22] K. Liu, J. Yan, M. S. Alam, and C. Zou, "Seismic fragility analysis of deteriorating recycled aggregate concrete bridge columns subjected to freeze-thaw cycles," *Engineering Structures*, vol. 187, pp. 1–15, 2019.

[23] Y. Xu, J. P. Wang, Y.-M. Wu, and H. Kuo-Chen, "Prediction models and seismic hazard assessment: a case study from Taiwan," *Soil Dynamics and Earthquake Engineering*, vol. 122, pp. 94–106, 2019.

[24] M. A. Zanini, L. Hofer, and C. Pellegrino, "A framework for assessing the seismic risk map of Italy and developing a sustainable risk reduction program," *International Journal of Disaster Risk Reduction*, vol. 33, pp. 74–93, 2019.

[25] F. Scozzese, A. Dall'Asta, and E. Tubaldi, "Seismic risk sensitivity of structures equipped with anti-seismic devices with uncertain properties," *Structural Safety*, vol. 77, pp. 30–47, 2019.

[26] G. Bartoli, M. Betti, L. Galano, and G. Zini, "Numerical insights on the seismic risk of confined masonry towers," *Engineering Structures*, vol. 180, pp. 713–727, 2019.

[27] R. D. Risia, A. Pennab, and A. L. Simonellib, "Seismic risk at urban scale: the role of site response analysis," *Soil Dynamics and Earthquake Engineering*, vol. 123, pp. 320–336, 2019.

[28] G. Andreotti and C. G. Lai, "Use of fragility curves to assess the seismic vulnerability in the risk analysis of mountain tunnels," *Tunnelling and Underground Space Technology*, vol. 91, p. 103008, 2020.

[29] H. Wang, F. Wang, H. Yang et al., "Time domain intrusive probabilistic seismic risk analysis of nonlinear shear frame structure," *Soil Dynamics and Earthquake Engineering*, vol. 136, p. 106201, 2020.

[30] Y. Liu, E. So, Z. Li et al., "Scenario-based seismic vulnerability and hazard analyses to help direct disaster risk reduction in rural Weinan, China," *International Journal of Disaster Risk Reduction*, vol. 48, Article ID 101577, 2020.

[31] R. Maio, J. M. C. Estêvão, T. M. Ferreira, and R. Vicente, "Casting a new light on the seismic risk assessment of stone masonry buildings located within historic centres," *Structures*, vol. 25, pp. 578–592, 2020.

[32] P. Castaldo and G. Alfano, "Seismic reliability-based design of hardening and softening structures isolated by double concave sliding devices," *Soil Dynamics and Earthquake Engineering*, vol. 129, Article ID 105930, 2020.

[33] S. Li, M. Zhang, W. Pei, Y. Lai, and W. Yu, "Thermo-seismic characteristics of a crushed-rock interlayer embankment on a permafrost slope," *Cold Regions Science and Technology*, vol. 151, pp. 249–259, 2018.

[34] C. Fan, H. Liu, J. Cao, and H. I. Ling, "Responses of reinforced soil retaining walls subjected to horizontal and vertical seismic loadings," *Soil Dynamics and Earthquake Engineering*, vol. 129, Article ID 105969, 2020.

[35] P. R. Jadhav and A. Prashant, "Computation of seismic translational and rotational displacements of cantilever retaining wall with shear key," *Soil Dynamics and Earthquake Engineering*, vol. 130, Article ID 105966, 2020.

[36] U. Yazgan, "Empirical seismic fragility assessment with explicit modeling of spatial ground motion variability," *Engineering Structures*, vol. 100, pp. 479–489, 2015.

[37] P. Foytong and T. Ornthammarath, "Empirical seismic fragility functions based on field survey data after the 5 may 2014 Mae Lao (Northern Thailand) earthquake," *International Journal of Disaster Risk Reduction*, vol. 42, Article ID 101344, 2020.

[38] V. E. Saouma and M. A. Hariri-Ardebili, "Seismic capacity and fragility analysis of an ASR-affected nuclear containment vessel structure," *Nuclear Engineering and Design*, vol. 346, pp. 140–156, 2019.

[39] I. Ioannou, R. E. Chandler, and T. Rossetto, "Empirical fragility curves: the effect of uncertainty in ground motion intensity," *Soil Dynamics and Earthquake Engineering*, vol. 129, p. 105908, 2020.

[40] J. Hu, J. Chen, Z. Chen et al., "Risk assessment of seismic hazards in hydraulic fracturing areas based on fuzzy comprehensive evaluation and AHP method (FAHP): a case analysis of Shangluo area in Yibin City, Sichuan province, China," *Journal of Petroleum Science and Engineering*, vol. 170, pp. 797–812, 2018.

[41] L. Tian, H. Pan, and R. Ma, "Probabilistic seismic demand model and fragility analysis of transmission tower subjected to near-field ground motions," *Journal of Constructional Steel Research*, vol. 156, pp. 266–275, 2019.

[42] D. Peduto, M. Korff, G. Nicodemo, A. Marchese, and S. Ferlisi, "Empirical fragility curves for settlement-affected buildings: analysis of different intensity parameters for seven hundred masonry buildings in The Netherlands," *Soils and Foundations*, vol. 59, no. 2, pp. 380–397, 2019.

[43] P. Castaldo, D. Gino, and G. Mancini, "Safety formats for non-linear finite element analysis of reinforced concrete structures: discussion, comparison and proposals," *Engineering Structures*, vol. 193, pp. 136–153, 2019.

[44] S. K. Chakrapani, "Nonlinear laminated plate theory for determination of third order elastic constants and acoustic nonlinearity parameter of fiber reinforced composites," *Composite Structures*, vol. 180, pp. 276–285, 2017.

[45] W. Ye, J. Liu, H. Fang, and G. Lin, "Numerical solutions for magneto-electro-elastic laminated plates resting on winkler foundation or elastic half-space," *Computers & Mathematics with Applications*, vol. 79, no. 8, pp. 2388–2410, 2020.

[46] C. Yin, F. F. Liu, and J. L. Zhang, "Seismic hazard assessment of Xi'an-baoji expressway," *Earthquake Engineering and Engineering Dynamics*, vol. 37, no. 2, pp. 181–188, 2017, (in Chinese).

[47] Z. Zheng, G. Hoogenboom, H. Cai, and Z. Wang, "Winter wheat production on the Guanzhong Plain of Northwest China under projected future climate with simCLIM," *Agricultural Water Management*, vol. 239, Article ID 106233, 2020.

[48] P. Castaldo and M. De Iuliis, "Effects of deep excavation on seismic vulnerability of existing reinforced concrete framed structures," *Soil Dynamics and Earthquake Engineering*, vol. 64, pp. 102–112, 2014.

[49] F. E. Udwadia and G. Di Massa, "Sphere rolling on a moving surface: application of the fundamental equation of

constrained motion," *Simulation Modelling Practice and Theory*, vol. 19, no. 4, pp. 1118–1138, 2011.
[50] S. Li, Y. Lai, M. Zhang, and W. Yu, "Seasonal differences in seismic responses of embankment on a sloping ground in permafrost regions," *Soil Dynamics and Earthquake Engineering*, vol. 76, pp. 122–135, 2015.
[51] M. Abyani, M. R. Bahaari, M. Zarrin, and M. Nasseri, "Effects of sample size of ground motions on seismic fragility analysis of offshore jacket platforms using genetic algorithm," *Ocean Engineering*, vol. 189, Article ID 106326, 2019.
[52] C. Bernier and J. E. Padgett, "Fragility and risk assessment of aboveground storage tanks subjected to concurrent surge, wave, and wind loads," *Reliability Engineering & System Safety*, vol. 191, Article ID 106571, 2019.
[53] B. Sun, S. Zhang, W. Cui, M. Deng, and C. Wang, "Nonlinear dynamic response and damage analysis of hydraulic arched tunnels subjected to P waves with arbitrary incoming angles," *Computers and Geotechnics*, vol. 118, Article ID 103358, 2020.
[54] H. K. Rad, H. Shariatmadar, and M. Ghalehnovi, "Simplification through regression analysis on the dynamic response of plates with arbitrary boundary conditions excited by moving inertia load," *Applied Mathematical Modelling*, vol. 79, pp. 594–623, 2020.
[55] T. Choudhury and H. B. Kaushik, "Treatment of uncertainties in seismic fragility assessment of RC frames with masonry infill walls," *Soil Dynamics and Earthquake Engineering*, vol. 126, Article ID 105771, 2019.
[56] B. Wei, Z. Hu, X. He, and L. Jiang, "Evaluation of optimal ground motion intensity measures and seismic fragility analysis of a multi-pylon cable-stayed bridge with super-high piers in mountainous areas," *Soil Dynamics and Earthquake Engineering*, vol. 129, Article ID 105945, 2020.
[57] V. Sangiorgio, G. Uva, and M. A. Aiello, "A multi-criteria-based procedure for the robust definition of algorithms aimed at fast seismic risk assessment of existing RC buildings," *Structures*, vol. 24, pp. 766–782, 2020.
[58] M. A. Jaimes and G. Candia, "Seismic risk of sliding ground-mounted rigid equipment," *Engineering Structures*, vol. 204, Article ID 110066, 2020.
[59] S. U. Khan, M. I. Qureshi, I. A. Rana, and A. Maqsoom, "An empirical relationship between seismic risk perception and physical vulnerability: a case study of Malakand, Pakistan," *International Journal of Disaster Risk Reduction*, vol. 41, Article ID 101317, 2020.
[60] H. X. Liu and Q. H. Zhang, "Characteristics of ground motion and earthquake damages," *Earthquake Research in China*, vol. 1, no. 1, pp. 35–40, 1985, (in Chinese).
[61] Y. Ao, K. Huang, Y. Wang, Q. Wang, and I. Martek, "Influence of built environment and risk perception on seismic evacuation behavior: evidence from rural areas affected by wenchuan earthquake," *International Journal of Disaster Risk Reduction*, vol. 46, Article ID 101504, 2020.
[62] D. Patsialis and A. A. Taflanidis, "Reduced order modeling of hysteretic structural response and applications to seismic risk assessment," *Engineering Structures*, vol. 209, Article ID 110135, 2020.
[63] P. Castaldo, B. Palazzo, and P. Della Vecchia, "Seismic reliability of base-isolated structures with friction pendulum bearings," *Engineering Structures*, vol. 95, pp. 80–93, 2015.
[64] P. Castaldo, B. Palazzo, T. Ferrentino, and G. Petrone, "Influence of the strength reduction factor on the seismic reliability of structures with FPS considering intermediate PGA/PGV ratios," *Composites Part B: Engineering*, vol. 115, pp. 308–315, 2017.
[65] A. Ramos, "Automatic differentiation for error analysis of Monte Carlo data," *Computer Physics Communications*, vol. 238, pp. 19–35, 2019.